Endoscopically guided spectral-domain OCT with double-balloon catheters

Wei Kang[1,3], Hui Wang[1,3], Yinsheng Pan[1], Michael W. Jenkins[1], Gerard A. Isenberg[2], Amitabh Chak[2], Matthew Atkinson[2], Deepak Agrawal[2], Zhilin Hu[1], and Andrew M. Rollins[1, 2*]

[1]*Department of Biomedical Engineering, Case Western Reserve University, 10900 Euclid Avenue, Cleveland, Ohio 44106, USA*

[2]*Department of Medicine, Case Western Reserve University, 10900 Euclid Avenue, Cleveland, Ohio 44106, USA*

[3]These authors contributed equally to this work

**rollins@case.edu*

Abstract: Fourier-domain optical coherence tomography (OCT) and balloon-based catheters have furthered the potential of OCT as a real-time surveillance tool for Barrett's esophagus (BE). However, a balloon catheter, which expands the esophagus and centers the catheter, applies direct pressure on the esophagus. This may affect the tissue appearance and the ability to detect dysplasia in BE. To study this effect, we propose a double-balloon catheter to allow imaging with and without balloon-tissue contact. A system design based on a spectral-domain OCT platform is reported and validated by acquisition of high quality, volumetric images of swine esophagus *in vivo*.

OCIS codes: (110.4500) Optical Coherence Tomography; (170.2150) Endoscopic imaging.

References and links

1. J. G. Fujimoto, M. E. Brezinski, G. J. Tearney, S. A. Boppart, B. E. Bouma, M. R. Hee, J. F. Southern, and E. A. Swanson, "Optical biopsy and imaging using optical coherence tomography," Nat. Med. **1**(9), 970–972 (1995).
2. G. J. Tearney, M. E. Brezinski, B. E. Bouma, S. A. Boppart, C. Pitris, J. F. Southern, and J. G. Fujimoto, "In vivo endoscopic optical biopsy with optical coherence tomography," Science **276**(5321), 2037–2039 (1997).
3. A. Sergeev, V. Gelikonov, G. Gelikonov, F. Feldchtein, R. Kuranov, N. Gladkova, N. Shakhova, L. Snopova, A. Shakhov, I. Kuznetzova, A. Denisenko, V. Pochinko, Y. Chumakov, and O. Streltzova, "In vivo endoscopic OCT imaging of precancer and cancer states of human mucosa," Opt. Express **1**(13), 432–440 (1997).
4. K. Kobayashi, J. A. Izatt, M. D. Kulkarni, J. Willis, and M. V. Sivak, Jr., "High-resolution cross-sectional imaging of the gastrointestinal tract using optical coherence tomography: preliminary results," Gastrointest. Endosc. **47**(6), 515–523 (1998).
5. B. E. Bouma, and G. J. Tearney, "Power-efficient nonreciprocal interferometer and linear-scanning fiber-optic catheter for optical coherence tomography," Opt. Lett. **24**(8), 531–533 (1999).
6. A. M. Rollins, R. Ung-Arunyawee, A. Chak, R. C. Wong, K. Kobayashi, M. V. Sivak, Jr., and J. A. Izatt, "Real-time in vivo imaging of human gastrointestinal ultrastructure by use of endoscopic optical coherence tomography with a novel efficient interferometer design," Opt. Lett. **24**(19), 1358–1360 (1999).
7. M. V. Sivak, Jr., K. Kobayashi, J. A. Izatt, A. M. Rollins, R. Ung-Runyawee, A. Chak, R. C. Wong, G. A. Isenberg, and J. Willis, "High-resolution endoscopic imaging of the GI tract using optical coherence tomography," Gastrointest. Endosc. **51**(4), 474–479 (2000).
8. B. E. Bouma, G. J. Tearney, C. C. Compton, and N. S. Nishioka, "High-resolution imaging of the human esophagus and stomach in vivo using optical coherence tomography," Gastrointest. Endosc. **51**(4), 467–474 (2000).
9. X. D. Li, S. A. Boppart, J. Van Dam, H. Mashimo, M. Mutinga, W. Drexler, M. Klein, C. Pitris, M. L. Krinsky, M. E. Brezinski, and J. G. Fujimoto, "Optical coherence tomography: advanced technology for the endoscopic imaging of Barrett's esophagus," Endoscopy **32**(12), 921–930 (2000).
10. S. Jäckle, N. Gladkova, F. Feldchtein, A. Terentieva, B. Brand, G. Gelikonov, V. Gelikonov, A. Sergeev, A. Fritscher-Ravens, J. Freund, U. Seitz, S. Schröder, and N. Soehendra, "In vivo endoscopic optical coherence tomography of esophagitis, Barrett's esophagus, and adenocarcinoma of the esophagus," Endoscopy **32**(10), 750–755 (2000).
11. G. Zuccaro, N. Gladkova, J. Vargo, F. Feldchtein, E. Zagaynova, D. Conwell, G. Falk, J. Goldblum, J. Dumot, J. Ponsky, G. Gelikonov, B. Davros, E. Donchenko, and J. Richter, "Optical coherence tomography of the esophagus and proximal stomach in health and disease," Am. J. Gastroenterol. **96**(9), 2633–2639 (2001).

#126994 - $15.00 USD Received 14 Apr 2010; revised 8 Jun 2010; accepted 29 Jun 2010; published 30 Jul 2010

12. J. M. Poneros, S. Brand, B. E. Bouma, G. J. Tearney, C. C. Compton, and N. S. Nishioka, "Diagnosis of specialized intestinal metaplasia by optical coherence tomography," Gastroenterology **120**(1), 7–12 (2001).
13. G. A. Isenberg, M. V. Sivak, Jr., A. Chak, R. C. Wong, J. E. Willis, B. Wolf, D. Y. Rowland, A. Das, and A. Rollins, "Accuracy of endoscopic optical coherence tomography in the detection of dysplasia in Barrett's esophagus: a prospective, double-blinded study," Gastrointest. Endosc. **62**(6), 825–831 (2005).
14. X. Qi, M. V. Sivak, G. Isenberg, J. E. Willis, and A. M. Rollins, "Computer-aided diagnosis of dysplasia in Barrett's esophagus using endoscopic optical coherence tomography," J. Biomed. Opt. **11**(4), 044010 (2006).
15. J. A. Evans, J. M. Poneros, B. E. Bouma, J. Bressner, E. F. Halpern, M. Shishkov, G. Y. Lauwers, M. Mino-Kenudson, N. S. Nishioka, and G. J. Tearney, "Optical coherence tomography to identify intramucosal carcinoma and high-grade dysplasia in Barrett's esophagus," Clin. Gastroenterol. Hepatol. **4**(1), 38–43 (2006).
16. J. A. Evans, B. E. Bouma, J. Bressner, M. Shishkov, G. Y. Lauwers, M. Mino-Kenudson, N. S. Nishioka, and G. J. Tearney, "Identifying intestinal metaplasia at the squamocolumnar junction by using optical coherence tomography," Gastrointest. Endosc. **65**(1), 50–56 (2007).
17. Y. Chen, A. D. Aguirre, P. L. Hsiung, S. Desai, P. R. Herz, M. Pedrosa, Q. Huang, M. Figueiredo, S. W. Huang, A. Koski, J. M. Schmitt, J. G. Fujimoto, and H. Mashimo, "Ultrahigh resolution optical coherence tomography of Barrett's esophagus: preliminary descriptive clinical study correlating images with histology," Endoscopy **39**(7), 599–605 (2007).
18. M. J. Cobb, J. H. Hwang, M. P. Upton, Y. Chen, B. K. Oelschlager, D. E. Wood, M. B. Kimmey, and X. D. Li, "Imaging of subsquamous Barrett's epithelium with ultrahigh-resolution optical coherence tomography: a histologic correlation study," Gastrointest. Endosc. **71**(2), 223–230 (2010).
19. G. W. Falk, T. W. Rice, J. R. Goldblum, and J. E. Richter, "Jumbo biopsy forceps protocol still misses unsuspected cancer in Barrett's esophagus with high-grade dysplasia," Gastrointest. Endosc. **49**(2), 170–176 (1999).
20. J. A. Jankowski, R. F. Harrison, I. Perry, F. Balkwill, and C. Tselepis, "Barrett's metaplasia," Lancet **356**(9247), 2079–2085 (2000).
21. S. H. Yun, G. J. Tearney, B. J. Vakoc, M. Shishkov, W. Y. Oh, A. E. Desjardins, M. J. Suter, R. C. Chan, J. A. Evans, I. K. Jang, N. S. Nishioka, J. F. de Boer, and B. E. Bouma, "Comprehensive volumetric optical microscopy in vivo," Nat. Med. **12**(12), 1429–1433 (2007).
22. B. J. Vakoc, M. Shishko, S. H. Yun, W. Y. Oh, M. J. Suter, A. E. Desjardins, J. A. Evans, N. S. Nishioka, G. J. Tearney, and B. E. Bouma, "Comprehensive esophageal microscopy by using optical frequency-domain imaging (with video)," Gastrointest. Endosc. **65**(6), 898–905 (2007).
23. M. J. Suter, B. J. Vakoc, P. S. Yachimski, M. Shishkov, G. Y. Lauwers, M. Mino-Kenudson, B. E. Bouma, N. S. Nishioka, and G. J. Tearney, "Comprehensive microscopy of the esophagus in human patients with optical frequency domain imaging," Gastrointest. Endosc. **68**(4), 745–753 (2008).
24. H. L. Fu, Y. Leng, M. J. Cobb, K. Hsu, J. H. Hwang, and X. Li, "Flexible miniature compound lens design for high-resolution optical coherence tomography balloon imaging catheter," J. Biomed. Opt. **13**(6), 060502 (2008).
25. A. F. Fercher, C. K. Hitzenberger, G. Kamp, and S. Y. El-Zaiat, "Measurement of intraocular distances by backscattering spectral interferometry," Opt. Commun. **117**(1-2), 43–48 (1995).
26. J. F. de Boer, B. Cense, B. H. Park, M. C. Pierce, G. J. Tearney, and B. E. Bouma, "Improved signal-to-noise ratio in spectral-domain compared with time-domain optical coherence tomography," Opt. Lett. **28**(21), 2067–2069 (2003).
27. R. Leitgeb, C. Hitzenberger, and A. Fercher, "Performance of fourier domain vs. time domain optical coherence tomography," Opt. Express **11**(8), 889–894 (2003).
28. M. Choma, M. Sarunic, C. Yang, and J. Izatt, "Sensitivity advantage of swept source and Fourier domain optical coherence tomography," Opt. Express **11**(18), 2183–2189 (2003).
29. J. Xi, L. Huo, Y. Wu, M. J. Cobb, J. H. Hwang, and X. Li, "High-resolution OCT balloon imaging catheter with astigmatism correction," Opt. Lett. **34**(13), 1943–1945 (2009).
30. V. Westphal, A. M. Rollins, J. Willis, M. V. Sivak, Jr., and J. A. Izatt, "Correlation of endoscopic optical coherence tomography with histology in the lower-GI tract," Gastrointest. Endosc. **61**(4), 537–546 (2005).
31. A. F. Peery, and N. J. Shaheen, "Optical coherence tomography in Barrett's esophagus: the road to clinical utility," Gastrointest. Endosc. **71**(2), 231–234 (2010).
32. Z. Hu, and A. M. Rollins, "Fourier domain optical coherence tomography with a linear-in-wavenumber spectrometer," Opt. Lett. **32**(24), 3525–3527 (2007).
33. W. Drexler, and J. G. Fujimoto, *Optical Coherence Tomography: Technology and Applications (Biological and Medical Physics, Biomedical Engineering)* (Springer, 2008), Chap. 32.
34. R. Huber, M. Wojtkowski, and J. G. Fujimoto, "Fourier Domain Mode Locking (FDML): A new laser operating regime and applications for optical coherence tomography," Opt. Express **14**(8), 3225–3237 (2006).
35. S. Yun, G. Tearney, J. de Boer, and B. Bouma, "Removing the depth-degeneracy in optical frequency domain imaging with frequency shifting," Opt. Express **12**(20), 4822–4828 (2004).
36. A. M. Davis, M. A. Choma, and J. A. Izatt, "Heterodyne swept-source optical coherence tomography for complete complex conjugate ambiguity removal," J. Biomed. Opt. **10**(6), 064005 (2005).
37. J. Zhang, J. S. Nelson, and Z. Chen, "Removal of a mirror image and enhancement of the signal-to-noise ratio in Fourier-domain optical coherence tomography using an electro-optic phase modulator," Opt. Lett. **30**(2), 147–149 (2005).
38. H. Wang, M. W. Jenkins, and A. M. Rollins, "A combined multiple-SLED broadband light source at 1300 nm for high resolution optical coherence tomography," Opt. Commun. **281**(7), 1896–1900 (2008).

#126994 - $15.00 USD Received 14 Apr 2010; revised 8 Jun 2010; accepted 29 Jun 2010; published 30 Jul 2010

39. Y. Chen, A. D. Aguirre, P. L. Hsiung, S. W. Huang, H. Mashimo, J. M. Schmitt, and J. G. Fujimoto, "Effects of axial resolution improvement on optical coherence tomography (OCT) imaging of gastrointestinal tissues," Opt. Express **16**(4), 2469–2485 (2008).
40. X. Qi, Department of Biomedical Engineering, Case Western Reserve University, Cleveland, Ohio 44106, Y. Pan, M. V. Sivak, Jr., J. E. Willis, G. A. Isenberg and A.M. Rollins, are preparing a manuscript to be called "Endoscopic Optical Coherence Tomography Image Analysis for Classification of Dysplasia in Barrett's esophagus."

1. Introduction

It has been shown that endoscopic OCT (EOCT) can obtain interpretable images of gastrointestinal (GI) mucosal microstructure, differentiate GI mucosal types and detect dysplasia in Barrett's esophagus (BE) [1–18]. These studies strongly suggest the feasibility of OCT as a screening and/or surveillance tool for BE, thereby augmenting the standard care consisting of GI endoscopy and tissue biopsy. Because the mucosal area involved in BE can be 20 cm^2 or more [19,20], recent EOCT work has focused on increasing the image acquisition speed and the field of view [21–24]. These improvements have enabled comprehensive imaging of segments of the esophagus in a clinically feasible time period (a few minutes). The key technologies enabling this improvement are Fourier-domain OCT (FD-OCT) for rapid image acquisition [25–28] and balloon catheters to dilate the lumen of the esophagus and center the fiber probe [21–24].

Previously reported balloon catheters for EOCT have been delivered to the esophagus using a guidewire or an overtube [22,29]. After delivery, the balloon was inflated to center the probe within an expanded lumen and held stationary while the probe was rotated and pulled back in a helical scan. However, the pressure on the mucosa caused by direct balloon-tissue contact may affect the appearance of the tissue in OCT images. We have previously shown that catheter pressure on colonic mucosa significantly alters the tissue appearance [30]. This raises the question of whether balloon pressure or contact affects OCT image features and dysplasia diagnosis in BE. To answer this question, a balloon-catheter-based EOCT platform must acquire comprehensive images with and without balloon-tissue contact. The platform must generate high quality OCT images rapidly in order to image segments of BE in patients. Also, the balloon-based catheter should be deployable through the accessory channel of the endoscope for user-friendly clinical procedures, endoscopic guidance of balloon positioning, correlation of endoscopic and OCT images, and documentation of biopsy and OCT imaging sites [31].

In this paper, we describe an EOCT platform for *in vivo* esophageal imaging that meets the requirements listed above. The system features a unique double-balloon catheter design. By scanning the beam between the two balloons, images without balloon-tissue contact can be obtained. Also the balloon design is capable of the conventional imaging through the balloon, and enables direct comparison of tissue appearance with and without balloon-tissue contact. This system furthermore represents the first demonstration of a balloon EOCT catheter deployable through the endoscope. In addition, this EOCT system is based on a spectral-domain OCT (SD-OCT) engine and shows comparable imaging performance to previously demonstrated esophageal EOCT systems which have all been based on swept light source OCT engines [21–24]. The system is validated by high quality, comprehensive imaging of swine esophagus *in vivo*, both with and without balloon-tissue contact.

2. Methods

2.1 EOCT System Design

The EOCT system schematic is shown in Fig. 1. It employs a 9.5 mW, broadband SLD light source (centered at 1310 nm) with a full-width-at-half-maximum (FWHM) bandwidth of 75 nm (IPSDM13xx, InPhenix, Inc., Livermore, CA). The measured axial resolution in air is 13 μm. The light was delivered through a circulator then split by a 90/10 fiber coupler. 90% of the light went to the sample arm, which consisted of a rotary-joint-pullback unit and a balloon catheter. 90% of the light collected from the sample arm was directed back through the circulator to the spectrometer for high power efficiency. The spectral interference fringes were

#126994 - $15.00 USD Received 14 Apr 2010; revised 8 Jun 2010; accepted 29 Jun 2010; published 30 Jul 2010

detected by a custom-designed, linear-in-wavenumber spectrometer, similar to the one previously described [32]. The spectrometer utilizes an InGaAs photodiode array line scan camera (SU-LDH 1024; SUI Goodrich, Princeton, NJ) with 1024 pixels and achieves a 4.2 mm imaging range. The –6dB falloff range occurs at 1.8mm. The pixel width of the camera is 25 µm. The optical resolution of the spectrometer is 13 µm. Finally, the detected spectrum was read by a frame grabber (NI PCIe-1427; National Instruments Corporation) which was synchronized to the rotation of the fiber probe. The image acquisition and display was coordinated by a custom software program written in C + + . The measured sensitivity of the system was 103dB.

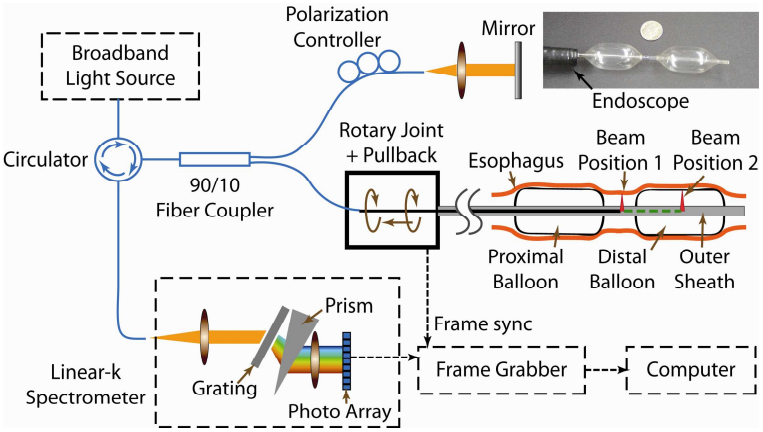

Fig. 1. System schematic of the double-balloon-based SD-EOCT system. Within the catheter, the beam can be located between two balloons for imaging without balloon-tissue contact (labeled beam position 1) or in a balloon for imaging with contact (labeled beam position 2). The inset photo (top right) shows the double-balloon catheter (compared with a dime) inserted through the GI endoscope and inflated.

2.2 Endoscopic balloon catheter

The endoscopic balloon catheter is a key component of the EOCT system and consists of three main parts, a fiber-optic probe, a rotary-joint-pullback unit and an outer sheath with balloons.

The fiber-optic probe is used to guide and focus the light onto the esophageal mucosa and to collect the image-bearing backscattered light. Figure 2(a) shows a mechanical model of the probe design (SolidWorks, Dassault Systèmes SolidWorks Corp., Concord, MA). A single-mode fiber (SMF28) was fixed in a ferrule followed by a glass spacer to expand the beam before entering a GRIN lens with a pitch of 0.295. A cylinder rod lens with a focal length of 12 mm was attached after the GRIN lens to correct the astigmatism induced by the outer sheath. All optical components have polished surfaces angled at 8 degrees to prevent back reflection. The lens group and ferrule were assembled into a glass tube and then glued into a metal housing. A gold mirror was glued at the tip of the metal housing to deflect the beam by 80 degrees relative the optical axis. Figures 2(b) and 2(d) are optical simulations (Zemax, ZEMAX Development Corp., Bellevue, WA) of the beam at a 9mm working distance without and with astigmatism correction, respectively. The corrected spot size was designed to be 30µm FWHM. Figures 2(c) and 2(e) show the beam at a 9 mm working distance before and after the astigmatism correction, respectively, as measured by a beam analyzer. The corrected spot had an ellipticity of 0.98 with a FWHM diameter of 33µm, which determines the transversal resolution and slice thickness of the images. The overall numerical aperture of the probe is 0.024. The total outer diameter of the fiber probe, including the metal housing, is 1.7 mm.

The rotary-joint-pullback unit generates a helical scanning pattern enabling volumetric imaging. The rotary-joint rotates the fiber probe to scan the esophagus circumferentially. The pullback system pulls the fiber probe, which is within the balloon catheter, slowly along the

#126994 - $15.00 USD Received 14 Apr 2010; revised 8 Jun 2010; accepted 29 Jun 2010; published 30 Jul 2010

longitudinal direction of the esophagus proximally towards the mouth. A 2m flexible tube encloses the optical fiber and transfers the torque and the force to the fiber probe. A transparent outer sheath was used to enclose the flexible tube while supporting the balloons. In order to be deployable through the GI endoscope, the diameter of the balloon catheter was restricted by the diameter of the accessory channel. The outer sheath had a diameter of 2.4 mm, which passed through the 3.6mm diameter channel with the balloon deflated.

The fiber probe was attached to the two necks of the balloon using biocompatible epoxy. The inflated balloons center the fiber probe in the esophageal lumen so that the beam from the fiber probe can maintain focus on the esophageal mucosa. The double-balloon design allows two imaging schemes to be employed in imaging the esophagus (with and without balloon-tissue contact). Figure 1 illustrates the double-balloon design. For imaging with no balloon-tissue contact, the images are obtained in the gap between the two balloons (labeled beam position 1). The fiber probe can also be placed within the distal balloon (labeled beam position 2) to acquire images through the balloon in the conventional way. Urethane low durometer balloons (18002501AC, Advanced Polymers Inc., Salem, NH) with a diameter of 18mm were utilized. The length of the gap was restricted to approximately 15mm to limit the extent of lumen contraction between the balloons, and keep the tissue within the axial imaging range. Holes were made in the outer sheath within the balloons so that they were inflated and deflated from the proximal end of the catheter.

2.3 Imaging protocol

The fiber probe was rotated at 10 revolutions per second and pulled back at 2 cm per minute. The incident light on the tissue was approximately 1 mW (6 mJ/cm^2, about 1% of the American National Standard Institute (ANSI) limit for skin exposure). The line scan camera acquired data at the full acquisition potential of 47k A-scans per second, which generated 95MB of raw data per second. Each frame consisted of 4,700 A-scans. The A-scan pitch was 11 µm at a 9 mm working distance and the frame pitch was 33 µm. 1 cm to 3 cm segments of esophagus were image.

The animal models were swine (20-40 kg) sedated with Telazol (8-12 mg/kg), intubated, ventilated and maintained under anesthesia with Isoflurane (1.5~2%) for the duration of the procedure. Heart rate and oxygen saturation was monitored. Intra-vascular access was gained and fluids were administered.

The endoscope was operated by gastroenterologists with experience in endoscopic surveillance of Barrett's esophagus (GAI, AC, MA, DA). An initial endoscopic inspection was performed with the OCT catheter hidden in the accessory channel. When a site was identified for imaging, the distal balloon was projected out of the accessory channel so that the gap between the balloons was visible. The fiber probe was placed under endoscopic guidance such that the probe beam passed between the two balloons. The endoscope was then pulled back 5 cm from the region of interest for deploying the proximal balloon, and both balloons were inflated. Volumetric images were obtained in the region of interest without balloon-tissue contact. Then the two balloons were deflated and the proximal balloon was pulled back into the accessory channel. The distal balloon and the probe beam were placed at the same region of interest under endoscopic guidance and the tissue was imaged with the balloon in contact with the tissue. A barometer was used to monitor the net balloon pressure, which did not exceed 0.5 atm at any time.

#126994 - $15.00 USD Received 14 Apr 2010; revised 8 Jun 2010; accepted 29 Jun 2010; published 30 Jul 2010

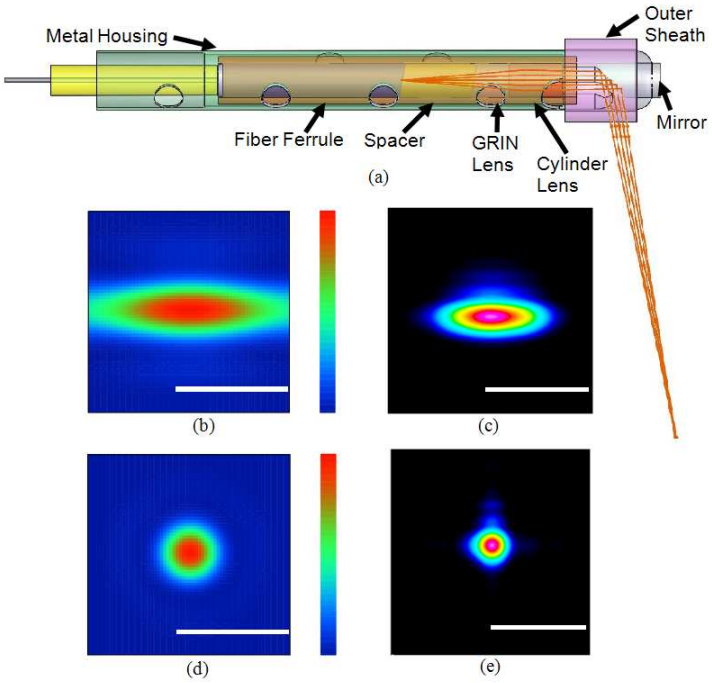

Fig. 2. (a) The mechanical design and optical design of the catheter. (b) & (d) Zemax simulations of the beam at the designed working distance without and with astigmatism correction, respectively. (c) & (e) Beam shapes without and with astigmatism correction, respectively, measured by a beam analyzer. Scale bars: 100 µm

3. Results

3.1 Endoscopically guided balloon deployment

Balloon deployment was accurately controlled endoscopically during the imaging procedure. Figure 3 is a single-frame excerpt from a video recording the operation of a balloon catheter in a swine esophagus *in vivo*. The tip of the fiber probe was clearly visible within the sheath so that its position could be adjusted. The entire balloon catheter was smoothly inserted through and pulled back into the accessory channel of the GI endoscope. The time required for balloon deployment was less than half a minute.

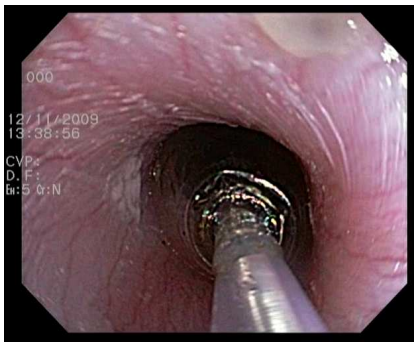

Fig. 3. One frame excerpted from a video recording (Media 1) demonstrating the insertion of the rotating fiber probe and inflation of the balloon in a swine esophagus in vivo. The diameters of the probe and the inflated balloon are 2.4 mm and 18 mm, respectively.

#126994 - $15.00 USD Received 14 Apr 2010; revised 8 Jun 2010; accepted 29 Jun 2010; published 30 Jul 2010

3.2 Swine esophageal imaging in vivo

We obtained comprehensive swine esophageal images *in vivo* with both double and single balloon imaging schemes as shown in Fig. 4. The diameters of the imaged esophagi were around 18 mm, but in order to visualize the tissue structure, the images are displayed with a diameter of about 3 mm. The scale bars indicate 1mm in the radial direction. Figure 4(a) is a representative cross-sectional image of the swine esophagus without balloon-tissue contact. The imaging depth in the tissue exceeds 1 mm and the tissue layers and structures can be clearly observed, including the squamous epithelium, lamina propria, muscularis mucosa, submucosa, muscularis propria, and blood vessels in the muscularis mucosa. Figure 4(b) shows a frame excerpted from a movie displaying volumetric visualization of a 17 mm long segment obtained within 50 seconds (approximately 5 GB of raw data). We observed that esophageal peristalsis caused distortion in the volumetric images along the longitudinal dimension. The distortion was corrected by segmenting the air-tissue interface and aligning the interface to a cylinder. Figures 4(c) and 4(d) show a representative cross-sectional image and the corresponding 3D reconstruction obtained with the single-balloon scheme (10 mm segment obtained within 30 seconds, approximately 3 GB of raw data). The typical layers of the esophagus can also be clearly recognized. The image signal is slightly stronger and more uniform than the non-contact image, but some structures (esp. blood vessels) are less apparent. The radial cropping magnifies the variance in the axial range of the tissue, and therefore the lumen appears more elliptical and/or eccentric in Figs. 4(a) and 4(c) than it would appear if the images were displayed with true aspect ratio.

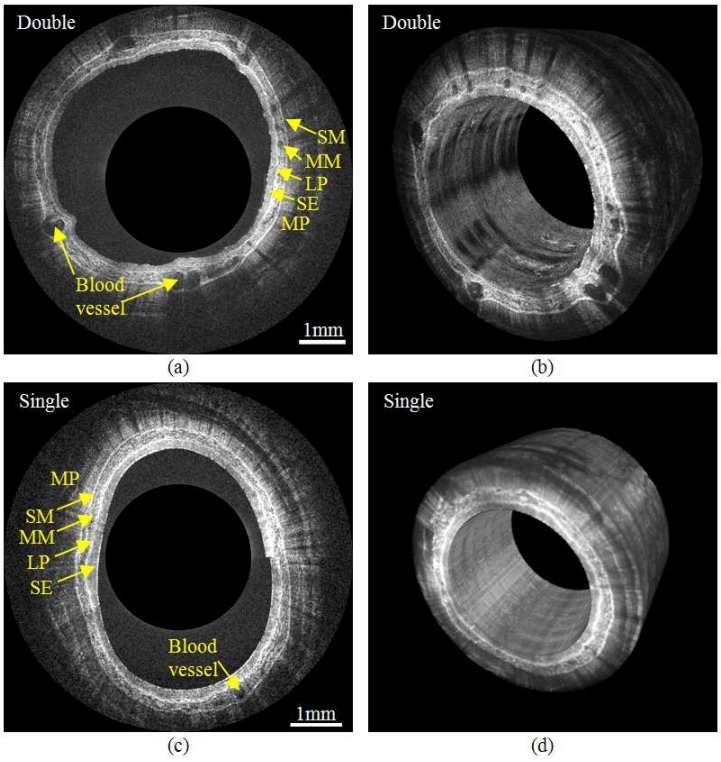

Fig. 4. (a) A representative cross-sectional image of a swine esophagus with the double-balloon imaging scheme. The layered structure that can be observed includes the squamous epithelium (SE), lamina propria (LP), muscularis mucosa (MM), submucosa (SM) and muscularis propria (MP). (b) One frame excerpted from a movie (Media 2) of a 17 mm long section of swine esophagus obtained with the double-balloon imaging scheme. (c) A representative cross-sectional image of the single-balloon imaging scheme. (d) 3D reconstruction of 10mm long segment with single-balloon imaging scheme

#126994 - $15.00 USD Received 14 Apr 2010; revised 8 Jun 2010; accepted 29 Jun 2010; published 30 Jul 2010

4. Discussion

The described endoscope-compatible double-balloon EOCT catheter allows imaging of the esophageal mucosa with and without direct balloon-tissue contact, which will allow us to study the influence of pressure on detection of dysplasia in BE. The two imaging schemes generate volumetric images of the esophagus rapidly without exchanging balloons. Deployment of the catheter through the endoscope is important because the two-scheme protocol is only possible with endoscopic visualization. Previous EOCT catheters, without balloons, were commonly designed for deployment through the endoscope [3,5–9,11,17]. Endoscope-guided deployment of an EOCT catheter bears advantages such as visual guidance and placement of the catheter, documentation of the procedure, and correlation of OCT and endoscopic views of the same tissue sites. It will also facilitate biopsy-correlation studies and, importantly, minimize the time added to the procedure when EOCT is employed in the clinic. Endoscopic deployment has not been demonstrated in previous reports of balloon-EOCT imaging [22,29]. A limitation of the current double-balloon EOCT system is that it is not designed to image arbitrarily long segments of BE. After investigating the consequences of balloon-tissue contact in BE surveillance, it will be necessary to design a probe capable of imaging long segments with optimum contact and pressure. In the demonstration presented here, the balloons were inflated to a larger diameter during double-balloon imaging than single-balloon imaging because the tissue within the gap has a smaller diameter than that supported by the balloons. Alternatively, if we find that it is important to maintain the balloons at a fixed diameter for a study, a shorter working-distance probe can be rapidly exchanged while the balloons remain in place in the esophagus.

The instrument reported here represents the first demonstration of a spectral-domain OCT system for gastrointestinal endoscopy. The usability of our SD-OCT system and image quality are comparable to previously demonstrated endoscopic swept light source OCT (SS-OCT) [21–24]. While SD-OCT is the conventional technology in retinal OCT imaging (which is the dominant clinical application of OCT imaging) [33], SS-OCT, also known as optical frequency domain imaging (OFDI), has been employed for all previous implementations of Fourier-domain OCT for endoscopy. There are several reasons for using SS-OCT. First, because of commercially available components, SD-OCT is more readily implemented than SS-OCT in the 830 nm range commonly used for retinal imaging, while at 1300 nm, commonly used in endoscopy, high quality components have been more readily available and more cost effective for SS-OCT than for SD-OCT. Rapidly scanning tunable lasers for SS-OCT were developed before fast line-scan cameras were available for SD-OCT at 1300 nm [21]. Furthermore, balloon-based EOCT requires a relatively long axial imaging range, to accommodate the axial position of the tissue which varies with radial position and moves due to peristalsis. SS-OCT more readily accomplishes long axial range because it generally benefits from less fall-off [34], can more easily resolve complex-conjugate ambiguity [35–37], and is not limited by a fixed number of spectral samples, as is SD-OCT. The endoscopic SD-OCT system reported here makes use of an InGaAs line-scan camera with 1024 pixels and a readout rate of 47,000 lines per second. This enabled SD-OCT that is not only fast enough for clinical pull-back procedures, but also has sufficient axial range (4.2 mm) to accommodate the variance of tissue position that we experienced in swine esophagus *in vivo*. InGaAs line-scan cameras appropriate for SD-OCT with more pixels and faster read-out will become available in the near future, further improving the feasibility of SD-OCT for endoscopic applications. The fall-off was improved by use of a linear-in-wavenumber spectrometer [32], and the probe optics was corrected to create a nearly Gaussian beam, so that high quality images are readily obtained. From these results and observations, we conclude that SD-OCT is a feasible alternative to SS-OCT for endoscopic imaging. We employed the SD-OCT configuration so that in the future we can incorporate our previously reported ultra-broadband light source into the EOCT system for improvement of the axial resolution (~5 μm) [38]. Ultrahigh resolution OCT reduces speckle size and enables visualization of finer morphological features in esophageal images, as previously reported in a time-domain

#126994 - $15.00 USD Received 14 Apr 2010; revised 8 Jun 2010; accepted 29 Jun 2010; published 30 Jul 2010

configuration [17,39], and may potentially benefit BE diagnosis. However, for a fixed-sized detector array, accommodating a broader bandwidth would trade-off with a shorter axial imaging range.

Some preliminary observations of the effects of balloon-tissue contact are apparent in Figs. 4(a) and 4(c). The natural mucosal surface topology is apparent in the double-balloon image, whereas the mucosal surface was compressed and smoothed by the balloon in the single-balloon image. The balloon-flattened surface resulted in more stable illumination and therefore more uniform image brightness. However, unpublished data has shown that surface topology may be useful for detecting dysplasia in BE [40]. Detailed structure in the muscularis mucosa, especially blood vessels, is more clearly observed in the double-balloon images. The imaging depth in the single-balloon images is greater, with multiple layers of muscularis propria visible, which is consistent with previous observations [30]. While we expected the double-balloon imaging scheme to result in higher variability of the axial position of the tissue as a function of radial position, the difference we observed was small, as seen in Fig. 4. However, the movement of the tissue due to peristalsis was greater with double-balloon imaging compared to single-balloon imaging. These observations suggest the need to further investigate the advantages and disadvantages of balloon-tissue contact and pressure, how tissue features in BE are altered, and how the changes affect detection of dysplasia in BE.

5. Conclusion

In conclusion, we have described an *in vivo* esophageal SD-OCT imaging platform that generates high quality volumetric images with double-balloon and single-balloon imaging schemes and endoscope-deployable catheters. We demonstrated imaging of swine esophagus using both schemes *in vivo* and presented preliminary observations. Future work includes evaluation of the imaging schemes in human patients, evaluation of the effects of balloon-tissue contact on detection of dysplasia in BE, and design of balloon-OCT catheters optimized for BE surveillance.

Acknowledgments

The authors acknowledge the contributions of Dr. Steve Schomisch in support of the swine experiments. The project described was support by the National Institute of Health grant numbers R03 EB004044-01, RO1 CA114276 and RO1 HL 083048. The content is solely the responsibility of the authors and does not necessarily represent the official views of the National Institutes of Health.

#126994 - $15.00 USD Received 14 Apr 2010; revised 8 Jun 2010; accepted 29 Jun 2010; published 30 Jul 2010